

# Two-qubit gate operations in superconducting circuits with strong coupling and weak anharmonicity

Xin-You Lü<sup>1,3</sup>, S. Ashhab<sup>1,2</sup>, Wei Cui<sup>1</sup>, Rebing Wu<sup>1,4</sup>, Franco Nori<sup>1,2</sup>

<sup>1</sup>Advanced Science Institute, RIKEN, Wako-shi, Saitama 351-0198, Japan

<sup>2</sup>Physics Department, The University of Michigan, Ann Arbor, Michigan 48109-1040, USA

<sup>3</sup>School of Physics, Ludong University, Yantai 264025, P. R. China

<sup>4</sup>Department of Automation, Center for Quantum information Science and Technology, Tsinghua University, Beijing, 100084, P.R. China

**Abstract.** We investigate theoretically the implementation of two-qubit gates in a system of two coupled superconducting qubits. In particular, we analyze two-qubit gate operations under the condition that the coupling strength is comparable to or even larger than the anharmonicity of the qubits. By numerically solving the time-dependent Schrödinger equation under the assumption of negligible decoherence, we obtain the dependence of the two-qubit gate fidelity on the system parameters in the case of direct and indirect qubit-qubit coupling. Our numerical results can be used to identify the “safe” parameter regime for experimentally implementing two-qubit gates with high fidelity in these systems.

PACS numbers: 03.67.-a; 42.50.Pq; 85.25.-j

## 1. Introduction

Superconducting (SC) circuits based on Josephson junctions are promising candidates for the realization of scalable quantum computing on a solid-state platform, due to their design flexibility, large-scale integration and controllability (see the reviews in Refs. [1, 2, 3, 4, 5, 6, 7]). SC qubits, include the charge [8], flux [9], and phase qubits [10, 11] as well as their variants, capacitively shunted flux qubits [12] and capacitively shunted charge qubits (transmon) [13]. The phase qubit, the capacitively shunted flux qubit and the transmon qubit are relatively insensitive to charge noise and can be operated over a wide range of parameters. Single-qubit gates [14], two-qubits gates [15, 16] and simple quantum algorithms [17] with these types of qubits have been demonstrated experimentally in recent years. However, comparing with the flux qubits, the common disadvantage of these types of qubits is their weakly-anharmonic energy level structure, i.e., the detuning between adjacent transition frequencies is very small.

Generally, the influence of the small anharmonicity (denoted by  $\Delta$ ) on quantum gate operations can be neglected when the qubit-field or qubit-qubit coupling strength is very small compared with  $\Delta$ . However, for the practical application of quantum computation, one wants to maximize the number of quantum gate operations with a given coherence time. In other words, we must implement quantum operations as fast as possible, which requires a strong qubit-qubit or qubit-field coupling to be employed during the single- and two-qubit gate operations [18]. The anharmonicity of SC qubits will influence the quality of quantum gates more and more with increasing coupling strength. Recently, there have been a number of theoretical studies analyzing the effects of weak anharmonicity of SC qubits on the operation of single-qubit gates and several optimization strategies have been proposed based on varying driving pulse shapes and sequences [19, 20, 21, 22, 23]. Similar to single-qubit gates, the weak anharmonicity of SC qubits will also influence the implementation of two-qubit gates. Then two questions arise naturally: (1) how much the weak anharmonicity of the qubits influence the implementation of two-qubit gates in a system of coupled SC qubits? (2) how strong can the coupling be while allowing a high two-qubit gate fidelity? In other words, how fast can two-qubit gates with high fidelity be implemented, given the weak anharmonicity of SC qubits?

Motivated by the above questions, in this paper we study the implementation of two-qubit gates with superconducting systems in the strong coupling regime. First, we introduce some possible methods for implementing two-qubit gates and qualitatively discuss the effect of strong coupling (section II). Then, in section III, we numerically simulate the influence of the coupling strength and anharmonicity on the fidelities of two-qubit gates in different superconducting systems, and show that the “safe” parameter regime for implementing two-qubit gates with high fidelity can be identified, which is useful for guiding experimental efforts based on superconducting qubits. Finally, we conclude with a brief summary in section IV.

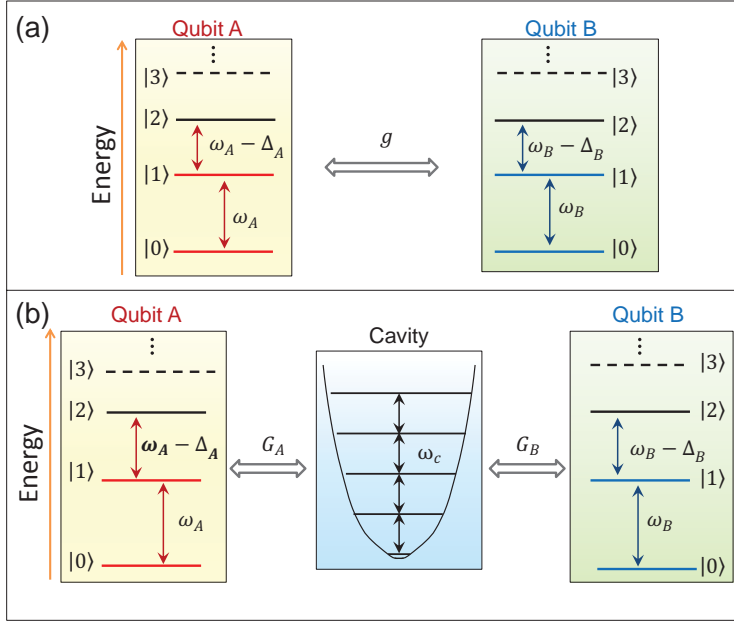


**Figure 1.** (Color online) System with direct (a) and indirect (b) qubit-qubit coupling. Here,  $g$ ,  $G_j$  and  $\Delta_j$  ( $j = A, B$ ) are the qubit-qubit, qubit-cavity coupling strength and anharmonicity, respectively.

## 2. Model and qualitative discussion

As shown in Fig. 1, as model systems we consider two directly (a) or indirectly (b) coupled SC qubits with weakly-anharmonic multilevel structure (such as transmon or phase qubits). Here it should be pointed out the flux qubits have a strong anharmonicity, and the problem discussed in this paper is not a serious limitation. The two lowest levels  $\{|0\rangle_j, |1\rangle_j\}$ , separated in energy by  $\hbar\omega_j$  ( $j = A, B$ ), are the computational basis, and the  $n$ th ( $n \geq 2$ ) higher levels are different from  $n\hbar\omega_j$  by  $\hbar\epsilon_n^j$ . Here  $\epsilon_n^j$  has the standard nonlinear oscillator form  $\epsilon_n^j = \Delta_j(n-1)n/2$  [24] and  $\Delta_j$  is the anharmonicity of the qubit, and it is positive in our paper.

In the case of direct qubit-qubit coupling, two qubits are directly (capacitively) coupled, while they are dispersively coupled to a common transmission line resonator in the case of indirect qubit-qubit coupling. The Hamiltonian of these two types of coupled system is given by ( $\hbar = 1$ ) [25, 26, 27, 28, 29, 30, 31, 32]

$$H^{direct} = \sum_{n=1}^{N-1} [(n\omega_A - \epsilon_n^A) |n\rangle_A \langle n| + (n\omega_B - \epsilon_n^B) |n\rangle_B \langle n|] + gJ_A^x \otimes J_B^{x,a}$$

$$H^{indirect} = \omega_c a^\dagger a + \sum_{j=A,B} \left[ \sum_{n=1}^{N-1} (n\omega_j - \epsilon_n^j) |n\rangle_j \langle n| + G_j (a + a^\dagger) J_j^x \right], \quad (1b)$$

$$J_A^x = \sum_{n=1}^{N-1} \eta_{n-1,n}^A \sigma_{n-1,n}^{Ax}, \quad J_B^x = \sum_{n=1}^{N-1} \eta_{n-1,n}^B \sigma_{n-1,n}^{Bx}, \quad (1c)$$

where  $H^d$  and  $H^{id}$  denote the Hamiltonian for the system with direct and indirect

qubit-qubit coupling,  $N$  is the number of levels in each SC qubit,  $\eta_{n-1,n}^j = \sqrt{n}$  is the level-dependent coupling matrix element, and  $\sigma_{n-1,n}^{jx} = |n-1\rangle_j\langle n| + |n-1\rangle_j\langle n|$  is the effective Pauli spin operators for levels  $|n-1\rangle$  and  $|n\rangle$ . Also,  $\omega_c$  is the frequency of the quantized cavity mode;  $g$  and  $G_j$  denote the qubit-qubit and qubit-cavity coupling strength.

In order to qualitatively analyze the implementation and fidelity of two-qubit gates, we assume that each qubit has three levels. Then, the Hamiltonian of direct qubit-qubit coupled system ( $H^{direct}$ ), under the rotation-wave approximation (RWA), can be reduced to

$$H_I^{direct} = \sum_{j=A,B} [\omega_j |1\rangle_j\langle 1| + (2\omega_j - \Delta_j) |2\rangle_j\langle 2|] + g[|01\rangle\langle 10| + \sqrt{2}|02\rangle\langle 11| + \sqrt{2}|20\rangle\langle 11| + 2|12\rangle\langle 21| + h.c.], \quad (2)$$

where  $|mn\rangle$  denotes  $|m\rangle_A|n\rangle_B$ .

For the system with indirect qubit-qubit coupling, under the dispersive qubit-cavity-coupling condition, i.e.,  $|\delta_j| = |\omega_j - \omega_c| \gg G_j$  ( $j = A, B$ ), the qubits will exchange energy by virtual photon processes. Then we can obtain the Hamiltonian of the effective qubit-qubit interaction by a Fröhlich transformation [33, 34, 35, 36],

$$H_{\text{eff},1}^{indirect} = \exp(-S)H^{id}\exp(S) \approx \sum_{j=A,B} \left\{ \left[ \left( \omega_j + \frac{G^2}{\delta_j} \right) |1\rangle_j\langle 1| + \left( 2\omega_j - \Delta_j + \frac{2G^2}{\delta_j - \Delta_j} \right) |2\rangle_j\langle 2| + \frac{G^2}{2\delta_j} a^\dagger a (|1\rangle_j\langle 1| - |0\rangle_j\langle 0|) + \frac{G^2}{\delta_j - \Delta_j} a^\dagger a (|2\rangle_j\langle 2| - |1\rangle_j\langle 1|) \right] + \left[ \frac{\sqrt{2}G^2}{2} \left( \frac{1}{\delta_j - \Delta_j} - \frac{1}{\delta_j} \right) a^2 |2\rangle_j\langle 0| + \frac{G^2}{2} \left( \frac{1}{\delta_A} + \frac{1}{\delta_B} \right) |01\rangle\langle 10| + \frac{\sqrt{2}G^2}{2} \left( \frac{1}{\delta_B - \Delta_B} + \frac{1}{\delta_A} \right) |02\rangle\langle 11| + \frac{\sqrt{2}G^2}{2} \left( \frac{1}{\delta_A - \Delta_A} + \frac{1}{\delta_B} \right) |20\rangle\langle 11| + G^2 \left( \frac{1}{\delta_A - \Delta_A} + \frac{1}{\delta_B - \Delta_B} \right) |12\rangle\langle 21| + h.c. \right] \right\}, \quad (3)$$

where

$$S = \sum_{j=A,B} \left[ \frac{G}{\delta_j} a^\dagger |0\rangle_j\langle 1| + \frac{\sqrt{2}G}{\delta_A - \Delta_A} a^\dagger |1\rangle_j\langle 2| - h.c. \right]. \quad (4)$$

Here, we have assumed that  $G_A = G_B = G$ .

The terms proportional to  $G^2$  in the first four terms of equation (3) represent level shifts, and the fifth term describes two-photon processes. Under the dispersive qubit-cavity-coupling condition, the cavity mode is only virtually excited during the gate operation, and therefore the third, fourth, and fifth terms of equation (3) vanish. Then, the Hamiltonian (3) can be simplified further as [37, 38, 39, 40, 41]

$$H_{\text{eff},2}^{indirect} = \sum_{j=A,B} [\tilde{\omega}_{j1} |1\rangle_j\langle 1| + (\tilde{\omega}_{j2} - \Delta_j) |2\rangle_j\langle 2|] + \left[ \sqrt{2}g_{\text{eff},1} |02\rangle\langle 11| + \sqrt{2}g_{\text{eff},2} |20\rangle\langle 11| + g_{\text{eff},3} |01\rangle\langle 10| + 2g_{\text{eff},4} |12\rangle\langle 21| + h.c. \right]. \quad (5)$$

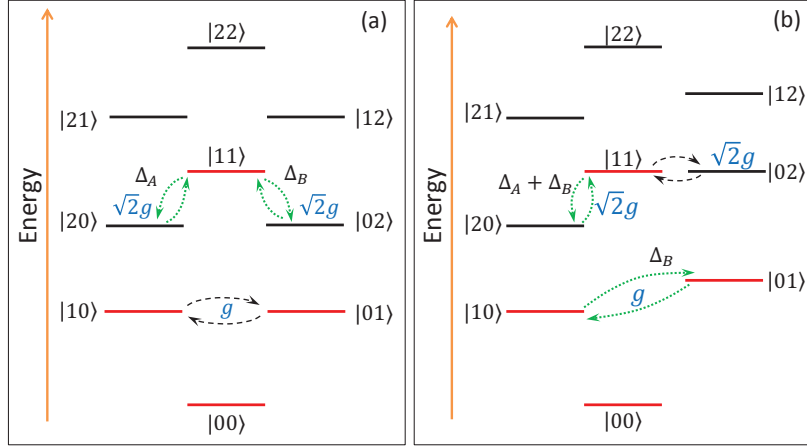


**Figure 2.** (Color online) The energy-level diagram of two-qubit product states for the iSWAP gate (a), and the controlled-Z gate (b) in the system with direct qubit-qubit coupling. Red levels denote the states in the computational basis. The black dashed arrows are the resonant transitions used for realizing the two-qubit gates and the green dotted arrows are the main *undesired* transitions, which adversely affect the implementation of two-qubit gates. The couplings  $g$  and  $\sqrt{2}g$  are indicated in blue, while the detuning between levels is indicated in black. This figure also applies the system with indirect qubit-qubit coupling when the corresponding couplings is replaced by  $g_{\text{eff},m}$  ( $m = 1, 2, 3, 4$ ).

where

$$\tilde{\omega}_{j1} = \omega_j + \frac{G^2}{\delta_j}, \quad (6a)$$

$$\tilde{\omega}_{j2} = 2\omega_j + \frac{2G^2}{\delta_j - \Delta_j}, \quad (6b)$$

$$g_{\text{eff},1} = \frac{G^2}{2} \left( \frac{1}{\delta_B - \Delta_B} + \frac{1}{\delta_A} \right), \quad (6c)$$

$$g_{\text{eff},2} = \frac{G^2}{2} \left( \frac{1}{\delta_A - \Delta_A} + \frac{1}{\delta_B} \right), \quad (6d)$$

$$g_{\text{eff},3} = \frac{G^2}{2} \left( \frac{1}{\delta_A} + \frac{1}{\delta_B} \right), \quad (6e)$$

$$g_{\text{eff},4} = \frac{G^2}{2} \left( \frac{1}{\delta_A - \Delta_A} + \frac{1}{\delta_B - \Delta_B} \right). \quad (6f)$$

Now, we obtain an effective interaction Hamiltonian similar to the Hamiltonian (2) in the system with direct qubit-qubit coupling.

From the Hamiltonians (2) and (5), it is easily seen that various two-qubit gates can be realized by appropriately adjusting the qubit frequencies ( $\omega_A, \omega_B$ ) both in the system with direct and indirect qubit-qubit coupling. For example, by setting  $\omega_A = \omega_B$  ( $\omega_B = \omega_A + \Delta_B$ ), the resonant transition between state  $|01\rangle$  and  $|10\rangle$  ( $|11\rangle$  and  $|02\rangle$ ) can be obtained as shown in Fig.2. Then the two-qubit iSWAP [15] (CZ [16, 17])

gate can be realized after an interaction time  $gt_g = \pi/2$  or  $g_{\text{eff},3}t_g = \pi/2$  ( $\sqrt{2}gt = \pi$  or  $\sqrt{2}g_{\text{eff},1}t = \pi$ ). Here it should be pointed out that some undesired transitions [see the (green) dotted arrows in Fig. 2] have been neglected in the weak-coupling regime  $g \ll |\Delta_j|$  or  $g_{\text{eff},m} \ll |\Delta_j|$  ( $m = 1 - 4; j = A, B$ ). However with increasing coupling strength  $g$  or  $g_{\text{eff},m}$ , the average amplitude  $g/|\Delta_j|$  or  $g_{\text{eff},m}/|\Delta_j|$  of undesired transitions will become larger and larger, which can not be neglected again and will reduce the fidelity of the two-qubit gate. So, the relative value of the coupling strength  $g$  or  $g_{\text{eff},m}$  and the anharmonicity  $\Delta_j$  is an important parameter for the quality of the two-qubit gate. In the two-qubit gate scheme based on SC qubits, a very strong qubit-qubit or qubit-cavity coupling strength cannot be employed due to the weak anharmonicity of the qubits, if one wants to obtain a high fidelity. How strong the coupling can be, while allowing high two-qubit-gate fidelities, will be analyzed in detail in the next section.

### 3. Numerical results

In this section, we will numerically calculate the fidelity of two-qubit gates in the circuits with either direct or indirect qubit-qubit coupling. Importantly, the present numerical results can help identify the safe parameter regime for implementing two-qubit gates with high fidelity. Here, we neglect the noise and decoherence of system in order to show explicitly the influence of coupling strength and anharmonicity on the fidelity of two-qubit gates. Here, it should also be pointed out that the single-qubit gates are performed using microwave pulses (with frequencies of a few of GHz), while the frequency tuning for the two-qubit gates are implemented using trapezoidal pulses.

Here, the fidelity of a two-qubit gate is defined as the Euclidean distance between the target  $U_T$  and the actual evolution  $U(t_g)$  [22],

$$F = 1 - \frac{1}{16} \|U_T - P^\dagger U(t_g) P\|_2^2, \quad (7)$$

where  $U(t)$  is the usual time evolution operator obeying the Schrödinger equation  $\dot{U}(t) = -\frac{i}{\hbar} H(t) U(t)$  in the full space of the quantum system. Here  $\|X\|_2^2 = \text{tr}(X^\dagger X)$  where  $X$  is an arbitrary operator.  $P$  is the projection operator on the two-qubit computational  $\{|00\rangle, |01\rangle, |10\rangle, |11\rangle\}$ ;

$$U_T = |00\rangle\langle 00| - i|01\rangle\langle 10| - i|10\rangle\langle 01| + |11\rangle\langle 11|$$

corresponds to the two-qubit iSWAP gate, and

$$U_T = |00\rangle\langle 00| + |01\rangle\langle 01| + |10\rangle\langle 10| - |11\rangle\langle 11|$$

corresponds to the two-qubit CZ gate. Here it should be pointed out that single-qubit rotations and an overall phase factor  $U_z^A = e^{i\theta_A \sigma_z^A}$ ,  $U_z^B = e^{i\theta_B \sigma_z^B}$ ,  $U_I = e^{i\theta I}$  are used in the numerical calculations in order to eliminate any extra phase factors;  $I$  is the unit matrix and

$$\sigma_z^A = |00\rangle\langle 00| + |01\rangle\langle 01| - |10\rangle\langle 10| - |11\rangle\langle 11|,$$

$$\sigma_z^B = |00\rangle\langle 00| - |01\rangle\langle 01| + |10\rangle\langle 10| - |11\rangle\langle 11|.$$

Specifically, in our numerical calculations, we replace the unitary operation  $U(t_g)$  in Eq. (7) by  $U'(t_g) = U_I U_z^B U_z^A U(t_g)$  and choose  $\theta_A$ ,  $\theta_B$  and  $\theta$  that maximize the fidelity.

We also note here that in our numerical calculations we do not use the RWA. But, there is almost no difference between these results shown below and the numerical results with the RWA (not shown in this paper). The reason is that the parameter regime that we consider does not reach the ultrastrong coupling regime and thus the RWA is valid here. Very recently, the influence of the counter-rotating terms in the Hamiltonian on the two-qubit gates in the ultrastrong coupling regime has been studied in a related system [42]. Also, the effect of counter-rotating terms were studied in [43].

### 3.1. System with direct qubit-qubit coupling

In this subsection, based on the original Hamiltonian Eq. (1a), we numerically calculate the influence of the coupling strength  $g$  and anharmonicity  $\Delta_j$  on the fidelities of the two-qubit iSWAP and CZ gates (see Figs. 3-5). Here we consider the two-qubit iSWAP and CZ gates implemented in experiments [15]. In Figs. 3(a) and (b), we plot the fidelities of the two-qubit iSWAP gate ( $F_{\text{iSWAP}}$ ) and the CZ gate ( $F_{\text{CZ}}$ ) as functions of  $g/\Delta_B$  in a circuit with direct qubit-qubit coupling, where we consider each SC qubit to have three levels (same approximation will be used in Figs. 4 and 5). From Fig. 3(a) and the (green) solid line in Fig. 3(b), it can be seen that the fidelities of these gates decrease with increasing  $g/\Delta_B$ , and the present numerical results can help identify the safe parameter regime for realizing two-qubit gates with high fidelities. As shown in Fig. 3(a), if we want to implement the two-qubit iSWAP (CZ) gate with fidelity higher than 99% (99.2%), the safe parameter regime is  $g/\Delta_B < 0.152$  ( $g/\Delta_B < 0.24$ ). In other words, based on the relationship  $gt_g = \pi/2$  for the iSWAP gate and  $\sqrt{2}gt_g = \pi$  for the CZ gate, the present numerical results can also identify the time limit for implementing two-qubit gates with high fidelity. For example, here the shortest gate time is  $t_g \approx 16.4$  ns ( $t_g \approx 12.9$  ns) for implementing a two-qubit iSWAP (CZ) gate with fidelity higher than 99% (99.2%).

The (green) solid line in Fig. 3(b) shows small oscillations in the fidelity of the two-qubit CZ gate. This result is due to the frequency mismatch between the undesired transitions and the resonant transition [see Fig. 2(b)], and it demonstrated that the fluctuations of the system parameters will influence the implementation of two-qubit gates. Based on the idea of adiabatically eliminating undesired transitions, these oscillations can be reduced by slowly adjusting the frequencies of the qubits during the gate operation. As shown in the inset of Fig. 3(b), the frequency of qubit B starts at  $1.1\omega_B$ , is first ramped down to  $\omega_B$  in  $\tau_d$ , then ramped up to  $1.1\omega_B$  after an interaction time  $t_g$  ( $\sqrt{2}gt_g = \pi$ ). During the full gate operation time ( $2\tau_d + t_g$ ), the frequency of qubit A is fixed. Using such pulses, we numerically calculate the fidelities of the two-qubit CZ gate for different values of  $\tau_d$  and present the results in Fig. 3(b) [See dashed, dotted and dot-dashed lines in Fig. 3(b)]. It can be seen that the oscillations of the

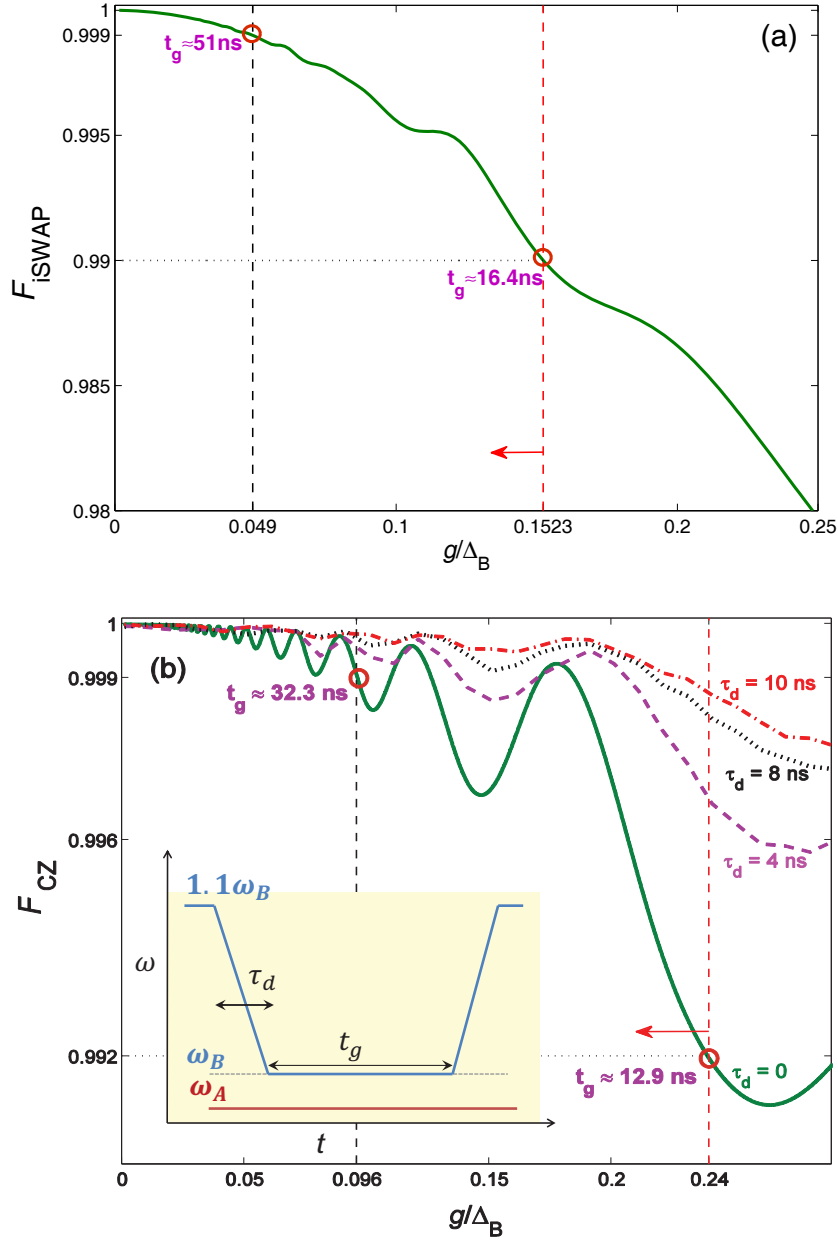


**Figure 3.** (Color online) The fidelities of the two-qubit iSWAP (a) and CZ (b) gate as functions of  $g/\Delta_B$  in a circuit with direct qubit-qubit coupling. Some representative dots are denoted by the dashed lines and red circles in order to present the relationship between the gate time  $t_g$  and fidelity  $F$ . The red arrows point out the parameter regime corresponding to two-qubit gate with high fidelity. In figure (b), the qubit frequencies are adiabatically adjusted during the gate operation, as shown in the inset part. The system parameters used here are: (a)  $\omega_A/2\pi = 5.5 \text{ GHz}$ ,  $\omega_B = \omega_A$ ,  $\Delta_A/2\pi = 0.15 \text{ GHz}$ , and  $\Delta_B/2\pi = 0.1 \text{ GHz}$ ; (b)  $\omega_A/2\pi = 7.16 \text{ GHz}$ ,  $\Delta_A/2\pi = 0.087 \text{ GHz}$ ,  $\Delta_B/2\pi = 0.114 \text{ GHz}$ , and  $\omega_B = \omega_A + \Delta_B$ .

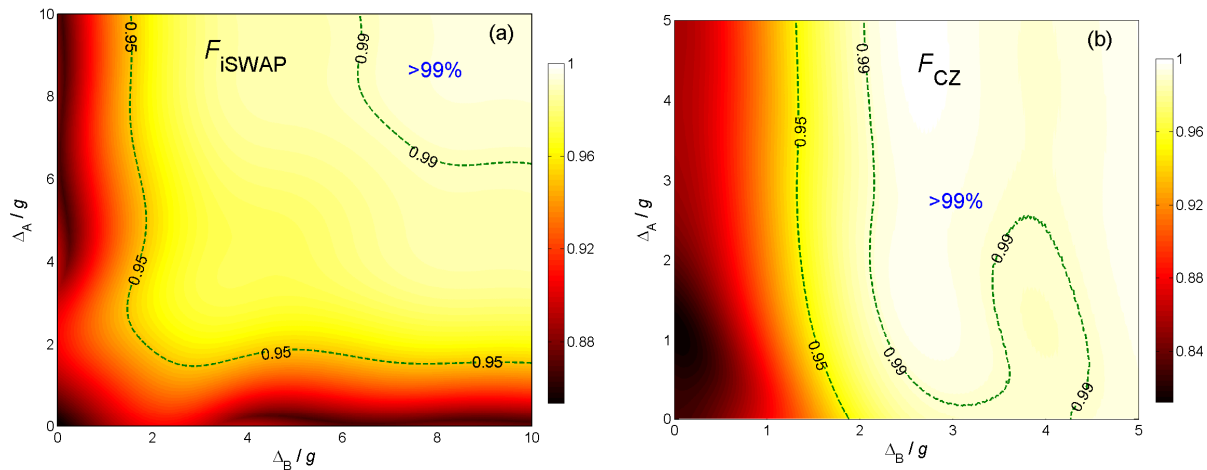


**Figure 4.** (Color online) The fidelities of the two-qubit iSWAP gate (a)  $F_{\text{iSWAP}}$  and CZ gate  $F_{\text{CZ}}$  (b) versus  $\Delta_A/g$  and  $\Delta_B/g$  in a circuit with direct qubit-qubit coupling. The dashed lines correspond to the parameter regime for implementing a two-qubit gate with fidelities 95% and 99%. The system parameters are the same as in Fig. 3 except for  $g/2\pi = 0.2$  GHz.

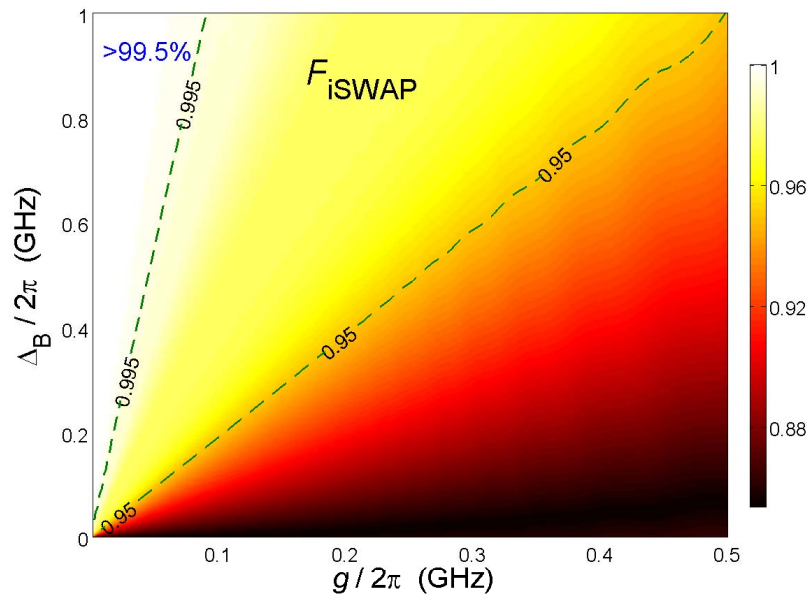


**Figure 5.** (Color online) The fidelities of the two-qubit iSWAP gates versus  $\Delta_B$  and  $g$  in a circuit with direct qubit-qubit coupling. The dashed lines correspond to the parameter regime for implementing two-qubit gate with fidelities 95% and 99.5%. The system parameters are the same as in Fig. 3 except for  $\Delta_A = \Delta_B$ .

fidelity can be eliminated by adiabatically adjusting the qubit frequencies during the gate operation. This numerical result provides a method to reduce the influence of parameter fluctuations on the implementation of two-qubit gates.

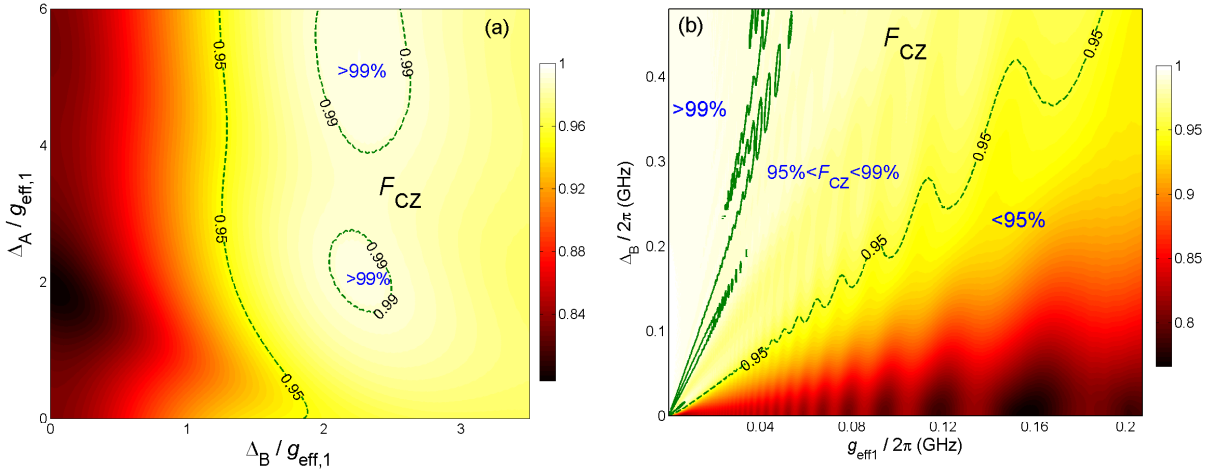


**Figure 6.** (Color online) The fidelity of the two-qubit CZ gate versus  $\Delta_A/g_{\text{eff},1}$ ,  $\Delta_B/g_{\text{eff},1}$  (a) and versus  $g_{\text{eff},1}$ ,  $\Delta_B$  (b) in the system with indirect qubit-qubit coupling. The dashed lines correspond to the parameter regime for implementing two-qubit gate with fidelities 95% and 99%. The basal system parameters are:  $\omega_c/2\pi = 6.9$  GHz,  $\omega_A/2\pi = 8.2$  GHz,  $\omega_B = \omega_A + \Delta_B$ ,  $\delta_j = \omega_j - \omega_c$  ( $j = A, B$ ); And  $G = 0.2$  GHz for panel (a),  $\Delta_A/2\pi = \Delta_B/2\pi$  GHz for panel (b).

In order to show the influence of  $\Delta_A$  and  $\Delta_B$  on the two-qubit gates, we plot the fidelities of the two-qubit iSWAP and CZ gates as functions of  $\Delta_A/g$  and  $\Delta_B/g$  in Fig. 4. It is easily seen from Fig. 4(a) that the anharmonicities  $\Delta_A$  and  $\Delta_B$  have equal effects on the two-qubit iSWAP gate, i.e., the larger the anharmonicities  $\Delta_j$  ( $j = A, B$ ) are, the higher the fidelity. This symmetric property disappears in the two-qubit CZ gate due to the asymmetry in the condition on the parameters,  $\omega_B = \omega_A + \Delta_B$  [see Fig. 4(b)]. In other words, the influence of the anharmonicity  $\Delta_A$  on the two-qubit CZ gate can be neglected when  $\omega_B = \omega_A + \Delta_B$  is chosen. In addition, the dashed lines in Fig. 4 indicate the safe regime of  $\Delta_j/g$  ( $j = A, B$ ) for implementing two-qubit iSWAP and CZ gates with fidelity higher than 99%.

In Figs. 3 and 4, either the anharmonicity  $\Delta_j$  or the coupling strength  $g$  have been set to a fixed value. A natural question is whether the conclusions obtained from Figs. 3 and 4 are universal. In other words, will the properties of Figs. 3 and 4 change much when either  $\Delta_j$  or  $g$  is changed? Thus, we now present in Fig. 5 three-dimensional (3D) plots of the dependence of  $F_{\text{iSWAP}}$  on  $g$  and  $\Delta_B$ . It is shown that the fidelity of two-qubit gates are approximately determined by the ratio of the qubit-qubit coupling strength  $g$  to the anharmonicity  $\Delta_j$  of the SC qubits. As a result, the conclusion obtained from Fig. 3(a) [or Fig. 4(a)] will not be changed when adjusting  $\Delta_B$  (or  $g$ ). A similar property is also obtained from the two-qubit CZ gate (the corresponding figures are not shown in this paper because are very similar to Fig. 5).

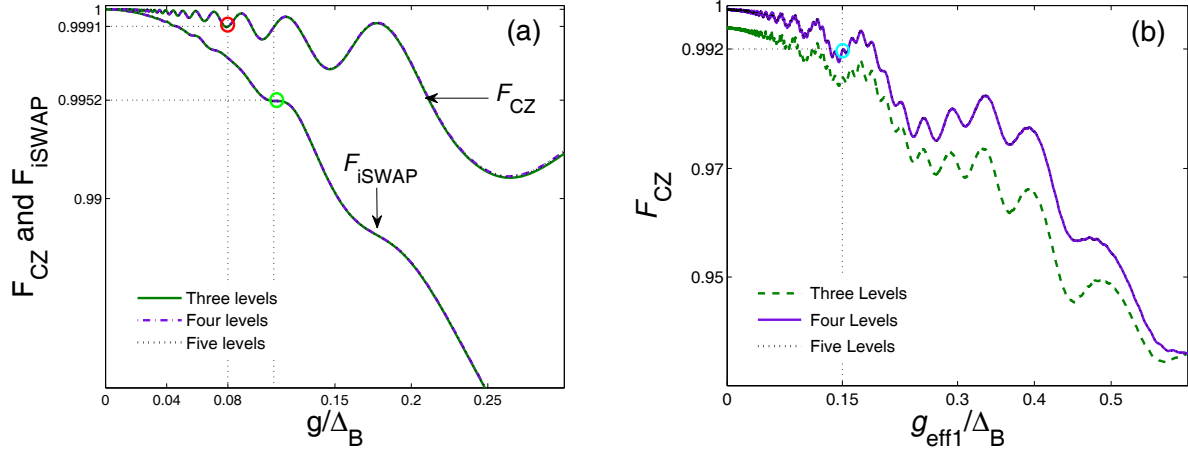


**Figure 7.** (Color online) The fidelities of the two-qubit gates as a function of  $g/\Delta_B$  (a) and  $g_{\text{eff},1}/\Delta_B$  (b) in systems with direct (a) and indirect (b) qubit-qubit coupling, when the three, four, or five lowest levels are considered for each qubit. The system parameters are the same as in Fig. 3 or 6. The green, red circles in (a) and cyan circle in (b) mark respectively the experimental parameters regime in Refs. [15], [16], [17].

### 3.2. System with indirect qubit-qubit coupling

In this subsection, based on the Hamiltonian Eq. (1b), we present the results of numerical calculations for the dependence of the fidelity of the two-qubit gates on the effective qubit-qubit coupling  $g_{\text{eff}1}$  and anharmonicity  $\Delta_j$  of SC qubits. Here the two-qubit CZ gates are realized based on the qubit-cavity dispersive interaction method [17], and the parameter

$$g_{\text{eff},1} = \frac{G^2}{2} \left( \frac{1}{\delta_B - \Delta_B} + \frac{1}{\delta_A} \right) = \frac{G^2}{\delta_A}$$

under the condition  $\omega_B = \omega_A + \Delta_B$ .

In Fig. 6, we present the 3D plots of the dependence of  $F_{CZ}$  on  $\Delta_A/g_{\text{eff},1}$  and  $\Delta_B/g_{\text{eff},1}$  [panel (a)], and  $g_{\text{eff},1}$  and  $\Delta_B$  [panel (b)], where we consider the SC qubits to have three levels. Using dashed lines, we have denoted the parameter regime for implementing two-qubit CZ gate with fidelities 95% and 99%. It is shown from Figs. 6(a) and (b) that high-fidelity areas correspond to the weak-coupling regime  $g_{\text{eff},1}/\Delta_j \ll 1$  ( $j = A, B$ ), while low fidelity corresponds to the strong-coupling regime, where  $g_{\text{eff},1}$  is comparable to or larger than  $\Delta_j$ . This property is similar as that in the system with direct qubit-qubit coupling. The present numerical results can be used to identify the safe parameter regime for implementing the two-qubit CZ gate with high fidelity in the circuit with indirect qubit-qubit coupling.

### 3.3. Going beyond the three-level approximation

Until now, three-level-system approximation for qubits has been used in the above numerical calculations. It is then natural to ask the following question: will our

conclusions, obtained from the above numerical results, still be valid for qubits with  $N$  ( $N > 3$ ) levels? To explore this, in Fig. 7, we plot the fidelities of the two-qubit iSWAP and CZ gates as functions of  $g/\Delta_B$  (or  $g_{\text{eff},1}/\Delta_B$ ) in the system with direct (or indirect) qubit-qubit coupling when each qubit has three, four or five levels. It can be seen from Fig. 7 that there is not much difference between the numerical results based on the three-, four- and five-level approximations for the qubits. So, our conclusions obtained from the above numerical calculations are still valid for  $N$ -level (with  $N > 3$ ) SC qubits.

### 3.4. Limits on the gate fidelities of recent experiments imposed by weak anharmonicity

In order to serve as a guide for future experiments, we compare our numerical results with corresponding experiments and show the limited fidelity of two-qubit gate based on SC qubits with weak anharmonicity. Based on the experimental parameters ( $\omega_A/2\pi$ ,  $\omega_B/2\pi$ ,  $\Delta_A/2\pi$ ,  $\Delta_B/2\pi$ ,  $g/2\pi$ ) equal to (5.5, 5.5, 0.15, 0.1, 0.011) GHz and (7.16, 7.274, 0.087, 0.114, 0.0091) GHz, two-qubit iSWAP [15] and CZ [16] gates with fidelities 63% and 70% were implemented in the circuit with direct qubit-qubit coupling. In the circuit with indirect qubit-qubit coupling, a two-qubit gate [17] with fidelity 85% was realized with system parameters ( $\omega_c/2\pi$ ,  $\omega_A/2\pi$ ,  $\omega_B/2\pi$ ,  $\Delta_A/2\pi$ ,  $\Delta_B/2\pi$ ,  $G_A/2\pi = G_B/2\pi$ ) equal to (6.9, 8.2, 8.45, 0.2, 0.25, 0.199) GHz. Corresponding to the above experimental parameters, in Fig. 7 we indicate the ideal fidelity (see the green, red and magenta circles) based on our theoretical calculations. From the comparison between experiments and our numerical calculations, we show that two-qubit gates with fidelities 99.52%, 99.91%, and 99.2% can be realized, in principle, if the influence of decoherence can be eliminated. Recently, the effects of decoherence on quantum gates and possible optimization routes were also studied in Ref. [44].

## 4. Conclusion

We have studied the performance of two-qubit gates in a system of two coupled SC qubits under the condition that the coupling strength is comparable to or larger than the anharmonicity of the qubits. First of all, by using the three-level approximation for the qubits, we analyzed and numerically calculated the dependence of the two-qubit gate fidelity on the qubit-qubit coupling strength and the anharmonicity of the qubits. Based on extensive numerical results, the safe parameter regime was identified for experimentally implementing two-qubit gates with high fidelity. Secondly, we numerically calculated the fidelity of the two-qubit gates in the case of four- and five-level approximations for the qubits, and demonstrated the validity of our numerical results for  $N$ -level qubits with  $N > 3$ . Our results can serve as a guide for future experiments based on SC qubits.

## Acknowledgments

We would like to thank E. Solano for useful discussions. This work was partially supported by ARO grant No. 0726909, JSPS-RFBR (No. 09-02- 92114), Grant-in-Aid for Scientific Research (S), MEXT Kakenhi on Quantum Cybernetics, the JSPS via its FIRST program. XYL was supported by the National Natural Science Foundation of China (Grant No. 11005057).

## References

- [1] You J Q and Nori F 2005 *Phys. Today* **58**(11) 42
- [2] Makhlin Y, Schön G, and Shnirman A 2001 *Rev. Mod. Phys.* **73** 357
- [3] Clarke J and Wilhelm F K 2008 *Nature* **453** 1031
- [4] Schoelkopf R J and Girvin S M 2008 *Nature* **451** 664
- [5] You J Q and Nori F 2011 *Nature* **474** 589
- [6] Buluta I and Nori F 2009 *Science* **326** 108
- [7] Buluta I, Ashhab S, and Nori F 2011 *Rep. Prog. Phys.* **74** 104401; Ladd T D, Jelezko F, Laflamme R, Nakamura Y, Monroe C, and O' Brien J L 2010 *Nature* **464** 45
- [8] Nakamura Y, Pashkin Y A, and Tsai J S 1999 *Nature* **398** 786
- [9] Van der Wal C H, Ter Haar A C J, Wilhelm F K, Schouten R N, Harmans C J P M, Orlando T P, Lloyd S, and Mooij J E 2000 *Science* **290** 773
- [10] Martinis J M, Nam S, Aumentado J, and Urbina C 2002 *Phys. Rev. Lett.* **89** 117901
- [11] Joo J, Bourassa J, Blais A, and Sanders B C 2010 *Phys. Rev. Lett.* **105** 073601
- [12] You J Q, Hu X, Ashhab S, and Nori F 2007 *Phys. Rev. B* **75** 140515(R); Steffen M, Kumar S, DiVincenzo D P, Rozen J R, Keefe G A, Rothwell M B, and Ketchen M B 2010 *Phys. Rev. Lett.* **105** 100502
- [13] Koch J, Yu T M, Gambetta J, Houck A A, Schuster D I, Majer J, Blais A, Devoret M H, Girvin S M, and Schoelkopf R J 2007 *Phys. Rev. A* **76** 042319
- [14] Martinis J M, Nam S, Aumentado J and Urbina C 2002 *Phys. Rev. Lett.* **89** 117901; Lucero E, Hofheinz M, Ansmann M, Bialczak R C, Katz N, Neeley M, O' Connell A D, Wang H, Cleland A N, and Martinis J M 2008 *Phys. Rev. Lett.* **100** 247001
- [15] Bialczak R C, Ansmann M, Hofheinz M, Lucero E, Neeley M, O'Connell A D, Sank D, Wang H, Wenner J, Steffen M, Cleland A N and Martinis J M 2010 *Nature Physics* **6** 409
- [16] Yamamoto T, Neeley M, Lucero E, Bialczak R C, Kelly J, Lenander M, Mariani M, O'Connell A D, Sank D, Wang H, Weides M, Wenner J, Yin Y, Cleland A N, and Martinis J M 2010 *Phys. Rev. B* **82** 184515; Chow J M, Córcoles A D, Gambetta J M, Rigett C, Johnson B R, Smolin J A, Rozen J R, Keefe G A, Rothwell M B, Ketchen M B, and Steffen M 2011 *Phys. Rev. Lett.* **107** 080502
- [17] DiCarlo L, Chow J M, Gambetta J M, Bishop L S, Johnson B R, Schuster D L, Majer J, Blais A, Frunzio L, Givin S M and Schoelkopf R J 2009 *Nature* **460** 240
- [18] Ashhab S, de Groot P C, Nori F 2012 *Phys. Rev. A* **85** 052327
- [19] Fazio R, Palma G M, and Siewert J 1999 *Phys. Rev. Lett.* **83** 5385
- [20] Steffen M, Martinis J M, and Chuang I L 2003 *Phys. Rev. A* **68** 224518
- [21] Zhou Z, Chu S I, and Han S 2005 *Phys. Rev. Lett.* **95** 120501
- [22] Reberstrost P, and Wilhelm F K 2009 *Phys. Rev. B* **79** 060507(R); Motzoi F, Gambetta J M, Reberstrost P, and Wilhelm F K 2009 *Phys. Rev. Lett.* **103** 110501
- [23] Ferrón A and Domínguez D 2010 *Phys. Rev. B* **81** 104505
- [24] Gambetta J M, Motzoi F, Merkel S T, and Willhelm F K 2011 *Phys. Rev. A* **83** 012308
- [25] You J Q, and Nori F 2003 *Phys. Rev. B* **68** 064509
- [26] Blais A, Huang R S, Wallraff A, Girvin S M, and Schoelkopf R J 2004 *Phys. Rev. A* **69** 062320

- [27] Ashhab S and Nori F 2007 *Phys. Rev. B* **76**, 132513 (2007).
- [28] Liu Y X, Wei L F, Tsai J S, and Nori F 2006 *Phys. Rev. Lett.* **96** 067003
- [29] Wu Y and Yang X 2007 *Phys. Rev. B* **76** 054425
- [30] Wu Y and Yang X 2005 *Phys. Rev. A* **71** 053806
- [31] Yamamoto T, Watanabe M, You J Q, Pashkin Y A, Astafiev O, Nakamura Y, Nori F, and Tsai J S 2008 *Phys. Rev. B* **77** 064505
- [32] Strauch F W, Johnson P R, Dragt A J, Lobb C J, Anderson J R, and Wellstood F C 2003 *Phys. Rev. Lett.* **91** 167005
- [33] Fröhlich H 1950 *Phys. Rev.* **79** 845
- [34] Sun C P 1990 *Phys. Rev. D* **41** 1318
- [35] Zhang H R, Cao Y B, Gong Z R, and Sun C P 2009 *Phys. Rev. A* **80** 062308
- [36] Ashhab S, Niskanen A O, Harrabi K, Nakamura Y, Picot T, de Groot P C, Harmans C J P M, Mooij J E, and Nori F 2008 *Phys. Rev. B* **77** 014510
- [37] Pellizzari T 1997 *Phys. Rev. Lett.* **79** 5242
- [38] Lü X-Y, Liu J-B, Ding C-L, and Li J-H 2008 *Phys. Rev. A* **78** 032305
- [39] Yang W, Xu Z, Feng M, and Du J 2010 *New J. Phys.* **12** 113039
- [40] Zheng S B, Yang Z B, and Xia Y 2010 *Phys. Rev. A* **81** 015804
- [41] Zhang J, Liu Y-X, Li C-W, Tarn T-J, and Nori F 2009 *Phys. Rev. A* **79** 052308
- [42] Wang Y M, Ballester D, Romero G, Scarani V, Solano E 2012 *Phys. Scr. T* **147** 014031; Romero G, Ballester D, Wang Y M, Scarani V, Solano E 2012 *Phys. Rev. Lett.* **108** 120501; Haack G, Helmer F, Mariantoni M, Marquardt F, and Solano E 2010 *Phys. Rev. B* **82** 024514
- [43] Cao X, You J Q, Zheng H, Kofman A G, Nori F 2010 *Phys. Rev. A* **82** 022119; Cao X, You J Q, Zheng H, Nori F 2011 *New J. Phys.* **13** 073002
- [44] Paladino E, Mastellone A, D'Arrigo A, and Falci G 2010 *Phys. Rev. B* **81** 052502; Paladino E, D'Arrigo A, Mastellone A, and Falci G 2011 *New J. Phys.* **13** 093037; D'Arrigo A, Paladino E 2012 *New Journal of Physics* **14** 053035